Comparison of Structurally-Related Alkoxide, Amine, and Thiolate-Ligated M (M= Fe, Co) Complexes: the Influence of Thiolates on the Properties of Biologically Relevant Metal Comple...

ARTICLE *in* INORGANICA CHIMICA ACTA · MARCH 2008

Impact Factor: 2.05 · DOI: 10.1016/j.ica.2007.07.038 · Source: PubMed

8 AUTHORS, INCLUDING:

Werner Kaminsky
University of Washington Seattle
282 PUBLICATIONS **3,867** CITATIONS
SEE PROFILE

Jason B Benedict
University at Buffalo, The State University o...
70 PUBLICATIONS **1,136** CITATIONS
SEE PROFILE

Julie A Kovacs
University of Washington Seattle
71 PUBLICATIONS **1,802** CITATIONS
SEE PROFILE

Available online at www.sciencedirect.com
ScienceDirect
Inorganica Chimica Acta xxx (2007) xxx–xxx
Inorganica Chimica Acta
www.elsevier.com/locate/ica

Comparison of structurally-related alkoxide, amine, and thiolate-ligated M^{II} (M = Fe, Co) complexes: The influence of thiolates on the properties of biologically relevant metal complexes

Lisa M. Brines, Gloria Villar-Acevedo, Terutaka Kitagawa, Rodney D. Swartz, Priscilla Lugo-Mas, Werner Kaminsky [1], Jason B. Benedict [1], Julie A. Kovacs *

Department of Chemistry, University of Washington, P.O. Box 351700, Seattle, WA 98195-1700, United States

Received 3 July 2007; accepted 31 July 2007

Dedicated to Edward Solomon

Abstract

Mechanistic pathways of metalloenzymes are controlled by the metal ion's electronic and magnetic properties, which are tuned by the coordinated ligands. The functional advantage gained by incorporating cysteinates into the active site of non-heme iron enzymes such as superoxide reductase (SOR) is not entirely understood. Herein, we compare the structural and redox properties of a series of structurally-related thiolate, alkoxide, and amine-ligated Fe(II) complexes in order to determine how the thiolate influences properties critical to function. Thiolates are shown to reduce metal ion Lewis acidity relative to alkoxides and amines, and have a strong *trans* influence thereby helping to maintain an open coordination site. Comparison of the redox potentials of the structurally analogous compounds described herein shows that alkoxide ligands favor the higher-valent Fe^{3+} oxidation state, amine ligands favor the reduced Fe^{2+} oxidation state, and thiolates fall somewhere in between. These properties provide a functional advantage for substrate reducing enzymes in that they provide a site at the metal ion for substrate to bind, and a moderate potential that facilitates both substrate reduction and regeneration of the catalytically active reduced state. Redox potentials for structurally-related Co(II) complexes are shown to be cathodically-shifted relative to their Fe(II) analogues, making them ineffective reducing agents for substrates such as superoxide.

Keywords: Synthetic thiolate-ligated iron complexes; Non-heme iron; X-ray crystal structures; Redox properties; Bioinorganic; Metalloenzyme function

1. Introduction

Cysteinate-ligated metalloenzymes and metalloproteins promote a number of critical biological processes [1–16]. Mechanistic pathways are controlled by the metal ion's electronic and magnetic properties, which are tuned by the coordinated ligands, and subtly altered by H-bonding interactions within the protein. Supporting ligands play an important role in determining function by controlling a metal ion's redox potential, as well as the basicity of bound substrates. Our group has put considerable effort into determining how coordinated cysteinate residues might control the chemistry taking place at the active-site of a metalloenzymes. Cysteinates are known to form highly covalent bonds to transition metals [17,18] and facilitate electron transfer reactions [19,20]. Our work has shown that thiolate ligands make low-spin iron accessible even in a non-heme environment [21–23], stabilize iron in the +3 oxidation state [21–23], and labilize sites *trans* to the thiolate thereby promoting reactivity by releasing product [24], even with low-spin Co(III) which is typically inert [25,26]. Recently, we showed that the thiolate ligand of a biomimetic superoxide reductase (SOR) model, $[Fe^{II}$-(cyclam-PrS)$]^+$, and its *trans* positioning relative to the

* Corresponding author.
E-mail address: kovacs@chem.washington.edu (J.A. Kovacs).
[1] UW staff crystallographers.

0020-1693/$ - see front matter © 2007 Elsevier B.V. All rights reserved.
doi:10.1016/j.ica.2007.07.038

substrate binding site, contribute significantly to the catalyst's function by dramatically lowering the Fe–O stretching frequency ($\nu_{Fe-O} = 419\ cm^{-1}$) and force constant ($k =$ 1.20 mdynes/cm) well-below that of any other reported iron-peroxo, thereby favoring Fe–O bond cleavage and H_2O_2 release [24]. Superoxide reductase, peptide deformylase, and nitrile hydratase occupy an unique niche amongst known non-heme enzymes in that they contain cysteinate ligands, as opposed to the more frequently encountered nitrogen and oxygen based ligands. The functional advantage gained by incorporating cysteinates is not entirely understood. By systematically replacing a single atom or functional group within identical ligand frameworks and comparing the structural and redox properties of the resulting iron complexes, we hope to address this question. For this purpose, we synthesized alkoxide and amine analogues of our functional SOR models $[Fe^{II}(S^{Me2}N_4(tren))]^+$ (**1**; tren = tris (2-aminoethyl)amine) and $[Fe^{II}(cyclam\text{-}PrS)]^+$ (**5**). Herein, we examine and compare the structures, and electronic, magnetic, and redox properties of this series of structurally related complexes. We also compare primary versus secondary versus tertiary amines, and structurally analogous Co(II) and Fe(II) complexes in order to determine how the metal ion, amine basicity, and steric bulk influences key properties critical to metalloenzyme function.

2. Experimental

2.1. General methods

All reactions were performed using standard Schlenk techniques under an atmosphere of dinitrogen. The iron complexes $[Fe^{II}(S^{Me2}N_4(tren))](PF_6)$ (**1**) [27], $[Fe^{II}(O^{Me2}N_4\text{-}(tren))(H_2O)](PF_6)$ (**2**) [28], $[Fe^{II}(cyclam\text{-}PrS)](BPh_4)$ (**5**) [24], and $[Fe^{II}(S^{Me2}N_4(tren\text{-}Et_4))]^+$ (**8**) [29], as well as 3-Boc-cyclam and cyclam-PrSAc · 4HCl [24], were synthesized as previously described. All other reagents were obtained from Aldrich and used without further purification. Solvents were purified through standard procedures [30]. 3-Methyl-3-mercapto-2-butanone was prepared according to a published procedure [23]. NMR spectra were recorded using Bruker AV-300, AV-301, or DPX 500 spectrometers and referenced to the residual protio solvent. ^1H NMR chemical shifts (δ) are reported in parts per million (ppm) and coupling constants (J) are reported in Hz. IR spectra were recorded on a Perkin-Elmer 1720 FT-IR. Electrospray mass spectra were recorded on a Bruker Esquire LC-Ion Trap Mass Spectrometer. EPR spectra were obtained using a Varian CW-EPR spectrometer at 4 K equipped with an Oxford helium cryostat. Cyclic voltammograms were recorded on a PAR 263A potentiostat with a glassy carbon working electrode, a platinum counter electrode, and Ag/Ag^+ (0.1 M) in acetonitrile as the reference electrode. Potentials were then converted to values referenced versus SCE. Electronic absorption spectra were recorded using a Hewlett–Packard 8453 diode array spectrometer. Magnetic moments were determined using a Quantum Design SQUID Magnetometer and by Evans' method as modified for a superconducting solenoid [31,32]. Temperatures were obtained using Van Geet's method [33]. Elemental analyses were performed by Galbraith Laboratories (Knoxville, TN) and Atlantic Microlab Inc. (Norcross, GA).

2.2. Synthesis of $[Fe^{II}(N^{Et2}N_4(tren))Cl](PF_6)$ (**3**)

A solution of *tris*(2-aminoethyl) amine (tren) (0.584 g, 4 mmol) was dissolved in 10 ml of dry methanol, followed by the addition of diethylaminoacetone (0.532 g, 4.00 mmol). This solution was allowed to stir for 10 min. Fe(II)Cl_2 (0.504 g, 4.00 mmol) was dissolved in 5 ml of dry methanol and added to the ligand mixture dropwise, immediately producing a yellow precipitate. $NaPF_6$ (1.34 g, 8.00 mmol) was added and the reaction mixture was allowed to stir overnight. The precipitate was filtered and washed with methanol to yield a pale yellow solid. Yield: 680 mg (53%). Yellow needle-like crystals were obtained by slow diffusion of diethyl ether into an acetonitrile solution. $E_{1/2}$ (MeCN, 298 K) = 303 mV versus SCE. Solution magnetic moment (303 K, MeCN) $\mu_{eff} =$ 5.37 BM. Magnetic moment in solid state: $\mu_{eff} = 5.23$ BM. Elemental *Anal.* Calc. for $FeN_5C_{13}H_{31}ClPF_6$: C, 31.63; N, 14.19; H, 6.33. Found C, 31.68; N, 14.17; H, 6.40%.

2.3. Synthesis of $[Co^{II}(S^{Me2}N_4(tren))](Cl)$ (**4**)

Anhydrous cobaltous chloride (519 mg, 4.00 mmol) in methanol (20 ml) was added dropwise to a solution containing $NaOCH_3$ (216 mg, 4.00 mmol), 3-methyl-3-mercapto-2-butanone (472 mg, 4 mmol), tren (585 mg, 4.00 mmol) and left to stir overnight. The resulting green solution was dried under reduced pressure, re-dissolved with a minimal amount of acetonitrile, and filtered through a fritted funnel. The solution was layered with diethyl ether and left to re-crystallize overnight giving pure **4** (700 mg, 52% yield) as a crystalline solid. Electronic absorption (CH_3CN): λ_{max} (ε) = 362 (1275) nm, 456 (243) nm, 504 (204) nm, 595 (179) nm. Redox potential (MeCN versus SCE): $E_{pa} = +270$ mV, $E_{pc} = -729$ mV. Elemental *Anal.* Calc. for $C_{11}H_{25}ClCoN_4S$: C, 38.88; H, 7.42; N, 16.49. Found: C, 38.64; H, 7.34; N, 16.69%.

2.4. Synthesis of CyclamPrOH · 4HCl

2.4.1. Synthesis of 3-iodo-1-propanol

To a 50 ml round bottom flask was added 3-chloro-1-propanol (2.93 g, 316 mmol) and sodium iodide (9.47 g, 632 mmol) in 20 ml acetone. The solution was refluxed overnight. After cooling to room temperature, the solution was filtered and the solvent was removed by rotary evaporation. The residue was redissolved in methylene chloride, filtered again, and the solvent was removed. The resulting red-orange oil was redissolved in 5 ml methylene chloride

Please cite this article in press as: L.M. Brines et al., Inorg. Chim. Acta (2007), doi:10.1016/j.ica.2007.07.038

and passed through a small silica plug (100% CH_2Cl_2). The first several fractions were collected and evaporated to give a brown oil (3.06 g, 52% yield). ^{1}H NMR ($CDCl_3$): 3.73 (q, 2H, $J = 5.70$ Hz), 3.30 (t, 2H, $J = 6.60$ Hz), 2.13 (s, 1H), 2.06 (quintet, 2H, $J = 6.00$ Hz).

2.4.2. Synthesis of 3Boc-cyclamPrOH

In a 50 ml round bottom flask was added 3-iodo-1-propanol (1.79 g, 9.62 mmol), 3Boc-cyclam (2.41 g, 4.81 mmol), and K_2CO_3 (1.33 g, 9.62 mmol) in 20 ml DMF. The solution was stirred under nitrogen at room temperature for 9 days. 100 ml of DI water was added to the solution and the product was extracted with ethyl acetate (3×30 ml). The organic layer was then washed with brine (2×30 ml) and dried over $MgSO_4$. Evaporation led to a sticky white residue of the product and excess 3-iodo-1-propanol. TLC revealed that the products would be difficult to separate, so the Boc deprotection step was carried out on the mixture. ESI-MS (M+1) calc. for M = $[N_4C_{28}H_{54}O_7]$: 558.7, found: 559.9.

2.4.3. Synthesis of CyclamPrOH · 4HCl

To the residue formed in the above step was added 15 ml of 4 M HCl/dioxane. The solution was allowed to stir at room temperature overnight. The solvent was removed by rotary evaporation and the residue was taken up in a MeOH/Et_2O solution (1:3). The solution was filtered and the precipitate was washed with additional ether (2×15 ml). The solid was further purified by triturating for 2 days in an Et_2O/CH_2Cl_2 mixture (1:1). The residue was then filtered, washed with additional ether, and pumped dry under vacuum. Yield: 1.92 g (~100%). ^{1}H NMR (D_2O): 3.65 (t, 2H, $J = 5.70$ Hz), 3.58–3.15 (m, 20H), 2.03 (m, 4H), 1.87 (m, 2H). ESI-MS (M+1) calc. for M = $N_4C_{13}H_{30}O$: 258.4; found: 259.3.

2.5. Synthesis of [Fe^{II}(cyclam-PrO)](BPh$_4$) · MeOH (6)

Sodium methoxide (270 mg, 5.00 mmol) and cyclam-PrOH · 4HCl (404 mg, 1.00 mmol) were dissolved in 15 ml methanol and allowed to stir for 30 min. A solution of $FeCl_2$ (127 mg, 1.00 mmol) in methanol (10 ml) was added dropwise to the ligand solution at room temperature. Sodium tetraphenylborate (342 mg, 1.00 mmol) was added and the solution was allowed to stir overnight. The solution was then filtered through Celite and the methanol was evaporated. The residue was redissolved in 20 ml acetonitrile and filtered again. The filtrate was concentrated to 10 ml, layered with ether (35 ml), and cooled to −40 °C to yield white solid **6**. Yield: 368 mg (58.2%). Single crystals suitable for X-ray diffraction were grown at room temperature over several days by layering ether (20 ml) onto a methanolic solution (10 ml) of **6**. ESI-MS calc. for $[FeN_4OC_{13}H_{29}]^+$: 313.2; found: 312.9. Magnetic moment (solid state): 4.79 BM. Redox potential (MeCN versus SCE): $E_{1/2} = +35$ mV. Elemental *Anal.* Calc. for $FeC_{38}H_{53}N_4O_2B$: C, 68.68; H, 8.04; N, 8.43. Found: C, 68.63; H, 7.93; N, 8.40%.

2.6. Synthesis of [Co^{II}(cyclam-PrS)][BPh$_4$] · MeCN (7)

Sodium methoxide (170 mg, 5.00 mmol) and cyclam-PrSAc · 4HCl (200 mg, 1.00 mmol) were dissolved in 15 ml of methanol, allowed to stir for 30 min and cooled to −30 °C. $CoCl_2 \cdot 6H_2O$ (82 mg, 1.00 mmol) was dissolved in 5 ml of methanol, cooled to −30 °C and added dropwise to the cold ligand while stirring. A pink solution instantly formed. Sodium tetraphenylborate (216 mg, 1.00 mmol) dissolved in 10 ml of methanol, was then added and the reaction mixture was stirred overnight. The solution was filtered, the filtrate was concentrated to 5 ml, layered with ether (25 ml) and cooled to −35 °C to yield pink crystals. Yield: 65 mg (46.5%). Electronic absorption (CH_3CN): λ_{max} (ε) = 324 (2029) nm, 366 (975) nm, 549 (116) nm; (MeOH) λ_{max} (ε) = 317 (2348) nm, 359 (1128) nm, 557 (134) nm. E_{pa} (MeCN) = +0.900 V versus SCE. Solution magnetic moment (310.2 K; MeOH) $\mu_{eff} = 3.97$ BM. EPR DCM/toluene glass (1:1), 10.3 K: $g_1 = 4.99$, $g_2 = 3.93$, $g_3 = 2.61$. ESI-MS cald. for $[CoN_4SC_{13}H_{29}]^+$: 332.8; found 332.2. Elemental *Anal.* Calc. for $CoC_{37}H_{49}N_4SB$: C, 66.30; N, 8.60; H, 7.62. Found C, 66.07, N, 8.43, H, 7.72%.

2.7. X-ray crystallography

A bi-refringent yellow crystal prism of **3** was cut down to $0.24 \times 0.12 \times 0.12$ mm and mounted on a glass capillary with oil. Data was collected at 23 °C on a Nonius Kappa CCD diffractometer. The crystal-to-detector distance was set to 30 mm and exposure time was 15 seconds per degree for all data sets with a scan width of 1.8°. The data collection was 98.6% complete to 24.71° in ϑ. A total of 20 518 partial and complete reflections were collected covering the indices, $h = -15$ to 16, $k = -21$ to 21, $l = -10$ to 10. Reflections (3472) were symmetry independent and the $R_{int} = 0.116$ indicated that the data was of less than average quality (average quality = 0.07). Indexing and unit cell refinements indicated an orthorhombic *P* lattice in the space group $Pna2_1$ (no. 33). Data was collected at room temperature because a slow splitting of peaks was observed upon cooling the crystal. The splitting of peaks appeared to indicate that a low temperature crystallographic phase transition was occurring, though no structure of this phase could be obtained. This does, however, explain the large thermal parameters of several atoms in the structure. Furthermore, the BASF parameter indicated the crystal was comprised of approximately 46% of the inversion twin of this structure.

A red prism, size $0.44 \times 0.38 \times 0.27$ mm of **4** was mounted on a glass capillary with oil. Data was collected at −143 °C. on a Nonius Kappa CCD diffractometer. The crystal-to-detector distance was set to 30 mm and exposure time was 15 seconds per degree for all data sets with a scan width of 2°. The data collection was 99.8% complete to 25° in ϑ. A total of 20 162 partial and complete reflections were collected covering the indices, $h = -13$ to 13, $k = -15$ to 17, $l = -15$ to 15. Reflections (3700) were

Table 1
Crystal data, intensity collections[a] and structure refinement parameters for $[Fe^{II}(N^{Et2}N_4(tren))(Cl)](PF_6)$ (**3**), $[Co^{II}(S^{Me2}N_4(tren))](Cl)$ (**4**), [Fe^{II}(cyclam-PrO)](BPh$_4$)MeOH (**6**), and [Co^{II}(cyclam-PrS)](BPh$_4$)MeCN (**7**)

	3	**4**	**6**	**7**
Formula	$FeC_{13}H_{31}ClF_6N_5P$	$CoC_{11}H_{25}ClNS$	$FeC_{38}H_{53}BN_4O_2$	$CoC_{39}H_{52}BN_5S$
MW	493.70	339.79	664.50	692.66
T (K)	296	130(2)	130(2)	130(2)
Unit cell	Orthorhombic	Monoclinic	Monoclinic	Monoclinic
a (Å)	13.6500(4)	10.3700(3)	8.1770(6)	9.2860(2)
b (Å)	18.6480(6)	12.9290(4)	12.7180(6)	19.6960(5)
c (Å)	8.575(1)	11.5130(4)	17.977(1)	21.3530(7)
α (°)	90	90	90	90
β (°)	90	94.654(1)	132.2251(8)	111.338(1)
γ (°)	90	90	90	90
V (Å^3)	2182.7(3)	1538.50(8)	3535.3(1)	1863.4(2)
Z	4	4	4	4
d(calc) (g/cm^3)	1.502	1.467	1.248	1.265
Space group	$Pna2_1$	$P2_1/c$	$P2_1/c$	$P2_1/c$
R	0.0500[b]	0.0443[b]	0.0548[b]	0.0553[b]
R_w	0.1284[c]	0.1180[c]	0.1549[c]	0.1238[d]
GOF	0.998	1.094	0.982	0.997

[a] Mo Ko(α, °) ($\lambda = 0.71070$ Å) radiation; graphite monochromator; −90 °C.
[b] $R = \Sigma||F_o| - |F_c||/\Sigma|F_o|$.
[c] $R_w = [\Sigma w(|F_o| - |F_c|)^2/\Sigma wF_o^2]^{1/2}$, where $w^{-1} = [\sigma^2_{count} + (0.05\,F^2)^2]/4F^2$.
[d] $R_w = \{\Sigma[w(F_o^2 - F_c^2)^2]/\Sigma[w(F_o^2)^2]\}^{1/2}$; $w = 1/[\sigma^2(F_o^2) + (0.1395P)^2 + 1.3703P]$, where $P = [F_o^2 + 2F_c^2]/3$.

Table 2
Selected geometrical parameters for the cations of $[Fe^{II}(S^{Me2}N_4(tren))](PF_6)$ (**1**), $[Fe^{II}(O^{Me2}N_4(tren))(H_2O)](PF_6)$ (**2**), $[Fe^{II}(N^{Et2}N_4(tren)(Cl))](PF_6)$ (**3**), $[Co^{II}(S^{Me2}N_4(tren))](Cl)$ (**4**), [Fe^{II}(cyclam-PrS)](BPh$_4$) (**5**), [Fe^{II}(cyclam-PrO)](BPh$_4$)MeOH (**6**), [Co^{II}(cyclam-PrS)](BPh$_4$) · MeCN (**7**), and $[Fe^{II}(S^{Me2}N_4$-(tren-Et$_4$))]$^+$ (**8**)

	1	**2**	**3**	**4**	**5**	**6**	**7**	**8**
M–X(S,O,N)	2.3281(9)	2.001(1)	2.293(5)	2.3006(7)	2.286(1)	1.906(2)	2.263(1)	2.3171(9)
M–N(1)	2.091(3)	2.129(2)	2.131(5)	2.050(2)	2.181(4)	2.225(2)	2.221(2)	2.104(3)
M–N(2)	2.268(3)	2.257(2)	2.267(5)	2.223(2)	2.138(4)	2.206(2)	2.099(3)	2.227(3)
M–N(3)	2.131(3)	2.249(2)	2.215(15)	2.086(2)	2.174(4)	2.151(2)	2.175(2)	2.219(3)
M–N(4)	2.117(3)	2.222(2)	2.232(14)	2.107(2)	2.166(4)	2.142(2)	2.086(3)	2.220(3)
M–L	N/A	2.149(1)	2.424 (2)	N/A	N/A	N/A	N/A	N/A
X–M–N(1)	84.02(8)	76.49(6)	75.1(2)	84.81(6)	101.2(1)	98.77(8)	99.07(7)	83.41(7)
X–M–N(2)	163.02(7)	153.14(6)	152.3(2)	163.96(6)	112.0(1)	95.70(8)	141.68(8)	161.53(7)
X–M–N(3)	108.8(8)	105.45(6)	107.0(6)	106.90(6)	104.9(1)	110.54(8)	91.29(8)	105.63(8)
X–M–N(4)	107.9(9)	108.00(6)	104.7(6)	112.4(2)	101.9(1)	121.16(8)	112.61(8)	109.64(7)
N(1)–M–N(2)	79.9(1)	76.71(7)	77.2(2)	79.49(8)	90.4(2)	165.45(8)	91.9(1)	78.6(1)
N(1)–M–N(3)	124.9(1)	94.77(6)	97.8(5)	125.14(8)	153.7(2)	92.37(8)	169.6(1)	121.4(1)
N(1)–M–N(4)	110.3(1)	103.51(7)	92.5(5)	122.54(8)	82.5(2)	82.21(8)	84.3(1)	111.4(1)
N(2)–M–N(3)	79.9(1)	78.57(7)	76.7(6)	79.93(8)	82.8(2)	81.09(9)	80.1(1)	81.3(1)
N(3)–M–N(4)	115.2(1)	144.73(7)	148.2(2)	102.54(8)	146.1(2)	128.26(8)	91.3(1)	118.49(9)
τ-value	0.64	N/A	N/A	0.65	0.13	0.62	0.47	0.67

Bond lengths and bond angles are given in Å and degrees, respectively.
X = S, N, or O.
L = sixth ligand (O or Cl).

symmetry independent and the $R_{int} = 0.0366$ indicated that the data was excellent (average quality = 0.07). Indexing and unit cell refinements indicated a monoclinic lattice in the space group $P2_1/c$ (no. 14).

A yellow crystal prism size $0.54 \times 0.34 \times 0.19$ mm of **6** was mounted on a glass capillary with oil. Data were collected at −143 °C on a Nonius Kappa CCD diffractometer. The crystal-to-detector distance was set to 30 mm and exposure time was 20 seconds per degree for all data sets with a scan width of 1.1°. The data collection was 99.0% complete to 25° in ϑ. A total of 78 675 partial and complete reflections were collected covering the indices, $h = -19$ to 18, $k = -12$ to 12, $l = -36$ to 43. Reflections (8278) were symmetry independent and the $R_{int} = 0.0829$ indicated that the data was of average quality (average quality = 0.07). Indexing and unit cell refinements indicated a primitive monoclinic lattice in the space group $P2_1/c$ (no. 14).

A purple crystal plate of **7** was cut down to $0.29 \times 0.12 \times 0.12$ mm and mounted on a glass capillary with oil. Data was collected at −143 °C on a Nonius

Kappa CCD diffractometer. The crystal-to-detector distance was set to 30 mm and exposure time was 40 seconds per degree for all data sets with a scan width of 1.6°. The data collection was 99.5% complete to 25° in ϑ. A total of 47402 partial and complete reflections were collected covering the indices, $h = -12$ to 12, $k = -23$ to 26, $l = -28$ to 28. Reflections (8679) were symmetry independent and the $R_{int} = 0.0738$ indicated that the data was of average quality (average quality = 0.07). Indexing and unit cell refinements indicated a primitive monoclinic lattice in the space group $P2_1/c$ (no. 14).

The data for **3**, **4**, **6**, and **7** were all integrated and scaled using HKL-SCALEPACK, and an absorption correction was performed using SORTAV. Solution by direct methods (SIR 97; default 4) produced complete heavy atom phasing models consistent with the proposed structures. All non-hydrogen atoms were refined anisotropically by full-matrix least-squares methods, while all hydrogen atoms were initially located in a difference Fourier map and were refined using a riding model. Crystal data for **3–4**, **6–7** is presented in Table 1. Selected bond distances and angles are assembled in Table 2.

3. Results and discussion

3.1. Synthesis of thiolate-, alkoxide-, and amine-ligated *1–8*

In order to correlate properties with metal ion structure and ligated atoms, one needs to compare structurally analogous systems in which only the heteroatoms or metal ion are varied and the ligand backbone remains the same. Multidentate ligands are generally required to maintain a somewhat rigid structure, since the biologically important first-row transition-metal ions tend to be substitution labile. Schematic drawings of the series of thiolate, alkoxide, and amine complexes described in this study are shown in Scheme 1.

Thiolate-ligated $[Fe^{II}(S^{Me2}N_4(tren))]^+$ (**1**) [27], $[Fe^{II}$-(cyclam-PrS)$]^+$ (**5**) [24], and $[Fe^{II}(S^{Me2}N_4(tren\text{-}Et_4))]^+$ (**8**) [29] were synthesized as previously described. Thiolate-ligated $[Co^{II}(S^{Me2}N_4(tren))](Cl)$ (**4**) and $[Co^{II}$ (cyclam-PrS)$]^+$ (**7**) were synthesized via a similar route using $CoCl_2$ or $[Co(H_2O)_6]Cl_2$ in place of $FeCl_2$. Thiolate-ligated **8**, which is a tertiary amine derivative of our functional SOR model **1**, was synthesized in order to determine if the amine N–H protons or H-atoms were involved in the proton-dependent mechanism of superoxide reduction. Alkoxide-ligated $[Fe^{II}(O^{Me2}N_4(tren))(H_2O)]^+$ (**2**) was synthesized as described elsewhere.[28] The cyclamPrOH · HCl ligand of alkoxide-ligated $[Fe^{II}$(cyclam-PrO)$]^+$ (**6**) was pre-assembled via a four step synthesis (outlined in Scheme 2), analogous to that previously reported for cyclam-PrSA-c · 4HCl [24]. For the sulfur-containing ligand, the thiolate must be protected (as a thioacetate group) throughout the synthesis to prevent oxidation of the thiol. For the alcohol-substituted ligand, no protecting group was needed for the alcohol. The alkoxide complex $[Fe^{II}$(cyclam-PrO)$]^+$ (**6**) was prepared via in situ deprotonation of the alcohol and amines using five equivalents of sodium methoxide, followed by the addition of $FeCl_2$ and $NaBPh_4$ in MeOH. Recrystallization from MeOH/Et_2O afforded analytically pure **6** as a white solid. The ESI-MS spectrum of this solid redissolved in methanol shows the major peak at $m/z = 312.9$, consistent with a 5-coordinate geometry for the iron-containing cation. This structure was confirmed by X-ray crystallography. Amine-ligated $[Fe^{II}(N^{Et2}N_4$-(tren)(Cl)$]^+$ (**3**) was synthesized via the $FeCl_2$-templated Schiff-base condensation between *tris* (2-aminoethyl)-amine) (tren) and diethylaminoacetone in MeOH.

3.2. Comparison of structures *1–8*

Single crystals of **3**, the Cl^- salt of **4**, **6**, and **7** were obtained via layer diffusion of Et_2O into an MeCN (**3**, **4**, **7**) or MeOH (**6**) solution. The structures of **1**, **2**, the PF_6^- salt of **4**, **5**, and **8** were described elsewhere [24,27–29]. Metrical parameters for **1–8** are compared in Table 2. ORTEP diagrams of **3**, **4**, **6**, and **7** are shown in Figs. 1 and 2. In contrast to the other structures, X-ray data for **3** was collected at ambient temperature because a phase change occurred at lower temperatures, thus the significantly larger thermal ellipsoids (Fig. 1). Alkoxide and amine-ligated

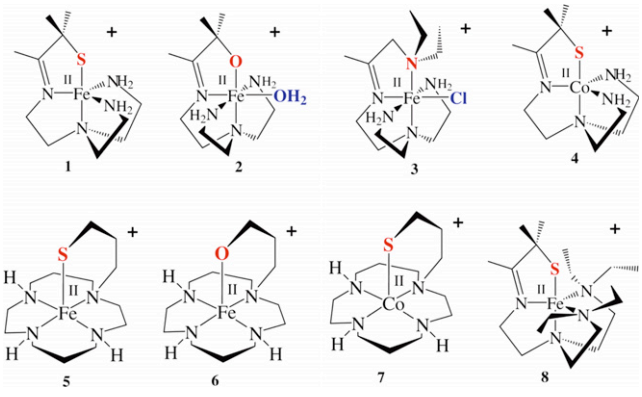

Scheme 1.

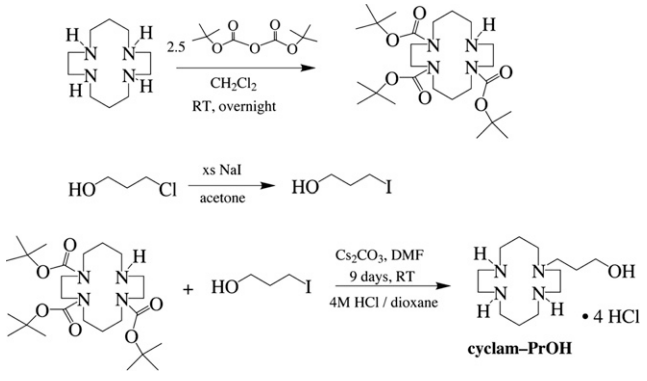

Scheme 2.

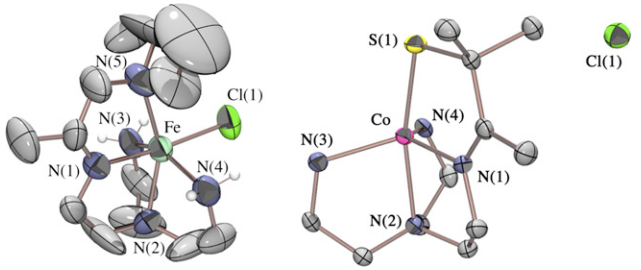

Fig. 1. ORTEP of $[Co^{II}(S^{Me2}N_4(tren))](Cl)$ (**4**) and the cation of $[Fe^{II}(N^{Et2}N_4(tren))(Cl)](PF_6)$ (**3**) showing that Cl^- binds to the amine-, but not the thiolate derivative. All hydrogen atoms, with the exception of the amine hydrogens, have been removed for clarity.

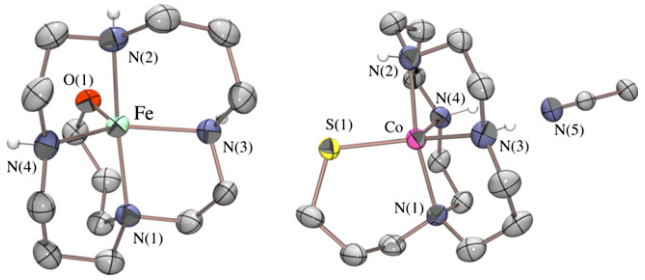

Fig. 2. ORTEP of the cations of $[Fe^{II}(cyclam\text{-}PrO)](BPh_4)$ (**6**) and $[Co^{II}(cyclam\text{-}PrS)](BPh_4) \cdot MeCN$ (**7**) showing the MeCN H-bonding to the N–H protons, but not coordinated to the metal ion of **7**. All hydrogen atoms, with the exception of the amine hydrogens, have been removed for clarity.

2 and **3** consistently crystallize as six-coordinate complexes with a water (**2**) or Cl^- (**3**) occupying the sixth site (Fig. 1, Scheme 1). In contrast, all of the thiolate-ligated complexes **1**, **4**, **5**, **7**, and **8** remain five-coordinate, even in the presence of coordinating solvents (MeCN, MeOH) or a Cl^- counterion. This suggests that the metal ion Lewis acidity is lower for thiolate-ligated **1**, **4**, **5**, **7**, and **8**, and greatest for amine and alkoxide-ligated **2** and **3**. The noticeable *trans* influence of the thiolate [25,34], as well as reduced molecular charge, could also be a factor partially responsible for the low coordination number. Amine-ligated **3** (Fig. 1) would be a dication if the Cl^- anion were not incorporated into its primary coordination sphere, explaining its higher affinity for Cl^-. This is in contrast to all of the other molecules included in this study in which charge is conserved to afford monocationic metal complexes. The fact that the Cl^- counterion is not incorporated into the primary coordination sphere of **4** (Fig. 1) can be attributed to a decreased Lewis acidity (relative to **3**) caused by the replacement of a neutral amine ligand with a monoanionic thiolate. Charge is conserved however, by replacing the thiolate of **1** with an alkoxide in **2**, and yet the alkoxide complex reproducibly binds a sixth ligand, whereas the thiolate complex **1** does not. Again this implies that the thiolate decreases the metal ion Lewis acidity helping to maintain an open coordination site. Thiolate-ligated **7** (Fig. 2) remains five-coordinate even though it cocrystallizes with a MeCN solvent. The acetonitrile nitrogen (N(5)) points directly towards the Co ion of **7**, is H-bonded to two of the cyclam secondary amine protons (N(5)H···N(3) = 2.245(9) Å; N(5)H···N(4) = 2.223(9) Å), and *trans* to the thiolate. These are not the first examples of coordinatively unsaturated thiolate complexes observed in our lab: our bis-thiolate-ligated iron complex $[Fe^{III}(S_2^{Me2}N_3(Pr,Pr))]^+$ remains five-coordinate even though it contains a more Lewis acidic Fe^{3+} metal ion, and the first-row series $[M^{II}(tren)N_4S^{Me2}]^+$ (M = Mn, Fe (**1**), Co, Ni, Cu, Zn) [16] all maintain five-coordinate structures even in coordinating solvents such as MeCN. These findings are unusual in that the synthesis of complexes containing an open-coordination site usually requires the use of steric bulk, non-coordinating solvents, and strict avoidance of potentially coordinating counterions [35–38].

Why alkoxide-ligated **6** does not bind a sixth ligand, whereas **2** does, is unclear. The secondary versus primary amines may be responsible (by lowering the metal ion Lewis acidity), although the redox potentials (vide infra) imply that this is not the case. Ligand constraints favoring a distorted trigonal bipyramidal geometry may also be involved. This was the explanation given for the consistently observed five-coordinate structure of the first-row tren-ligated $[M^{II}(tren)N_4S^{Me2}]^+$ (M = Mn, Fe (**1**), Co, Ni, Cu, Zn) series recently reported by our group [16]. The fact that alkoxide and amine-ligated tren complexes **2** and **3** afford six-coordinate structures would appear to rule this out. On the other hand, it may be that the cyclam ligand of **6** constrains the geometry to be five-coordinate when a metal ion that is too large to fit inside the macrocyclic cavity is involved. The high spin Fe^{2+} ion of **6** (vide infra) would be larger than the preferred low-spin Fe^{2+}, or oxidized Fe^{3+}.

With the exception of **5**, the five-coordinate structures are all tetragonally distorted trigonal bipyramidal ($\tau = 0.47$–0.67) approximately half-way between square pyramidal ($\tau = 0.0$) and trigonal bipyramidal ($\tau = 1.0$). Thiolate-appended cyclam-ligated **5** is much closer to square pyramidal ($\tau = 0.13$). The X = S, O, N heteroatom occupies the apical position of the tren-derived complexes (**1**, **4**, and **8**), and the equatorial plane of the cyclam-derived complexes **6** and **7**. The Co^{II}-cyclam complex **7** crystallizes as the less frequently encountered *trans*-V (*R*,*R*,*R*,*R*) isomer, whereas **5** and **6** are both isolated as the more common *trans*-I (*R*,*S*,*R*,*S*) isomer. The *trans*-I configurational isomer is the most stable isomer for five-coordinate cyclam complexes.

For the five-coordinate structures, the alkoxide Fe–O bond (1.906(2) Å in **6**) is significantly shorter than the thiolate Fe–S bonds (range: 2.286(1) Å (in **5**) – 2.3281(9) Å (in **1**)), as one would expect based on differences between the covalent radii of O versus S. The alkoxide Fe–O bond (2.001(1) Å) for the six-coordinate structure **2** is longer than that of the five-coordinate structure **6**, as expected based on the size difference of 5- versus 6-coordinate metal ion radii [39]. The tertiary amine Fe–N(5) bond of **3**

(2.293(5) Å) is longer than the tertiary amines of five-coordinate **5** (2.181(4) Å), **6** (2.225(2) Å), and **8** (mean: 2.222(5) Å), most likely because it is six-coordinate. Within the tren-ligated systems, there is less variability of these tertiary amine distances (range: 2.223(2)–2.268(3) Å) most likely due to ligand constraints. The secondary amine Fe–N distances (2.138Å in **5** to 2.206(2) in **6**) are noticeably shorter than the tertiary amine Fe–N bonds, but longer than the imine Fe–N bonds, and the primary amine Fe–N bonds (2.117 Å and 2.131(3) Å in **1**). The Co–S, Co–O, and Co–N distances in **4** and **7** are noticeably shorter than those of their iron analogues. This is expected based on periodic trends [16].

3.3. Comparison of the electronic and magnetic properties of *1–8*

In contrast to the intensely colored, low-spin Fe(III)-thiolates, the Fe(II)-thiolates **1**, **5**, and **8** described herein are pale in color, and high-spin, due to the absence of charge transfer bands in the visible region, and the absence of pentet excited states. There is a poorer energy match between the reduced metal ion d- and sulfur-orbitals, so these charge transfer bands fall outside the visible region. The alkoxide and amine complexes **2**, **3**, and **6** are pale yellow and high-spin. The pale color of these solutions is due to the weak intensity of Laporte-forbidden d–d transitions for the six-coordinate complexes, or poor energy match between the metal ion d- and alkoxide-orbitals. The thiolate-ligated cobalt complexes **4** and **7** are slightly more intensely colored due to the presence of lower energy charge transfer bands that tail into the visible (Fig. 3 and supplemental Figure S-4). The charge transfer bands are lower in energy for Co^{2+} because the more electronegative metal ion's orbitals lie lower than those of Fe^{2+}. The electronic absorption spectra of **1** and **4–8** are all solvent-independent implying that solvents do not bind to the metal ion's open coordination site, even in coordinating solvents.

The iron complexes **1** [40], **2** [28], **3** ($\mu_{eff} = 5.23$ BM; Fig. 4), **5**, [24] **6** ($\mu_{eff} = 4.79$ BM; Figure S-2), and **8** [29] are all high-spin $S = 2$ both in the solid state and in solution. This is irrespective of whether the fifth ligand X (Table 2) is an alkoxide, thiolate, or amine (Fig. 4). The cobalt complexes **4** ($\mu_{eff} = 4.05$ BM), [16] and **7** ($\mu_{eff} = 3.97$ BM; supplemental) are both high-spin as well with an $S = 3/2$ ground state over the temperature range 4–300 K.

3.4. Comparison of redox potentials – correlation with apical ligand X (*S, O, N*) and metal ion (Co^{2+}, Fe^{2+})

Upon oxidation, the iron and cobalt complexes **1** and **4** both have been shown to convert to low-spin ($S = 1/2$ or 0) six-coordinate M^{3+} structures [27,41]. The iron complex, $[Fe^{II}(S^{Me2}N_4(tren))]^+$ (**1**), reacts with HO_2 to afford six-coordinate $[Fe^{III}(S^{Me2}N_4(tren))(MeCN)]^{2+}$ via a hydroperoxo intermediate $[Fe^{III}(S^{Me2}N_4(tren))(OOH)]^+$ [27,42]. Cyclic voltammograms of **3**, **6**, and **7**, are shown in

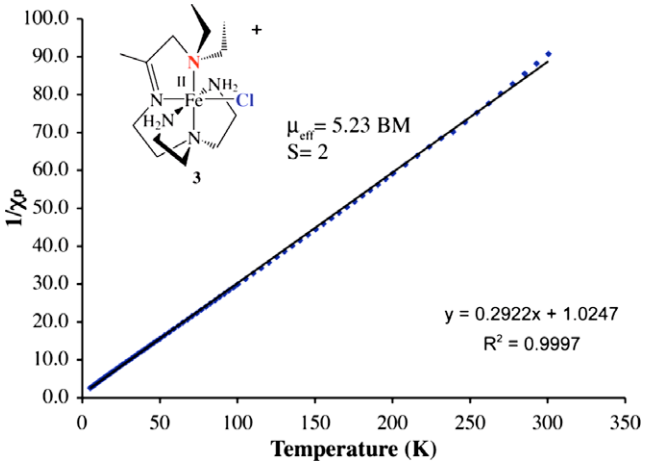

Fig. 4. Inverse molar magnetic susceptibility ($1/\chi_m$) vs. temperature (T) plot for $[Fe^{II}(N^{Et2}N_4(tren))(Cl)](PF_6)$ (**3**) fit to an $S = 2$ spin-state.

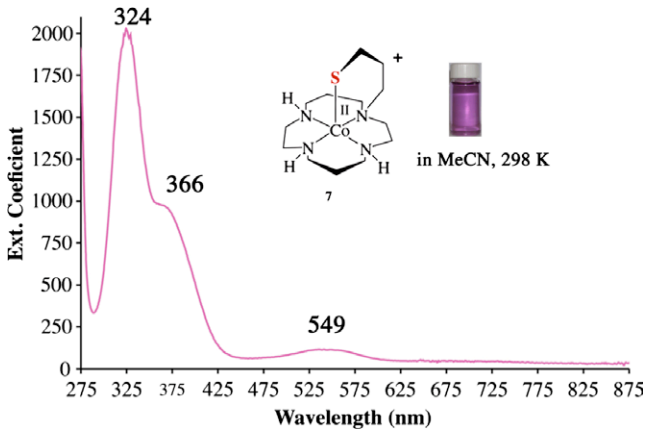

Fig. 3. Electronic absorption spectrum of $[Co^{II}(cyclam\text{-}PrS)](BPh_4)\cdot MeCN$ (**7**) in MeCN at ambient temperature.

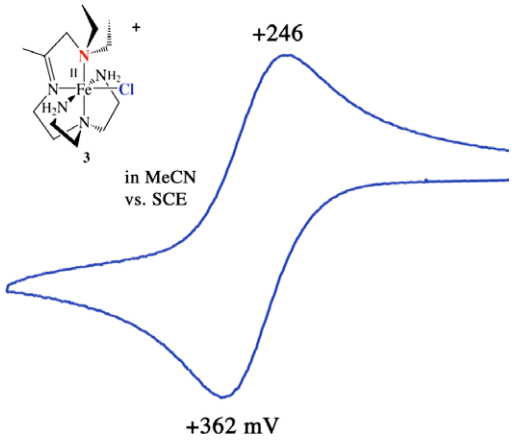

Fig. 5. Cyclic voltammogram of $[Fe^{II}(N^{Et2}N_4(tren))(Cl)](PF_6)$ (**3**) in MeCN at 298 K (0.1 M $(Bu_4N)PF_6$, glassy carbon electrode, 150 mV/s scan rate). Peak potentials versus SCE indicated.

Table 3
Comparison of redox potentials for thiolate, alkoxide, and amine-ligated M(II) complexes

	$E_{1/2}$ (vs SCE) (mV)
$[Fe^{II}(S^{Me2}N_4(tren))]^+$ (**1**)	−200
$[Fe^{II}(S^{Me2}N_4(tren\text{-}Et_4))]^+$ (**8**)	+410 (E_{pa}, irrev.)
$[Fe^{II}(O^{Me2})N_4(tren)(H_2O)]^+$ (**2**)	−285 (pH = 6.8, E_{pa}, irrev.)
	−420 (pH = 10.6, E_{pa}, irrev.)
$[Fe^{II}(N^{Et2}N_4(tren)(Cl))]^+$ (**3**)	+303
$[Co^{II}(S^{Me2}N_4(tren))]^+$ (**4**)	+270 (E_{pa}, irrev.)
$[Fe^{II}(cyclam\text{-}PrS)]^+$ (**5**)	+135
$[Fe^{II}(cyclam\text{-}PrO)]^+$ (**6**)	+35
$[Fe^{II}(cyclam)(MeCN)_2]^{2+}$	+700
$[Co^{II}(cyclam\text{-}PrS)]^+$ (**7**)	+900 (E_{pa}, irrev.)

Fig. 5, and supplemental Figs. S-6 and S-7, respectively. Redox potentials are assembled in Table 3. Comparison of the redox potential ($E_{1/2}$ and E_{pa}; Table 3) of tren-ligated **1** versus that of tren-ligated **4** [16] shows that replacement of the Fe^{2+} with Co^{2+} within an identical ligand environment causes the potential to shift cathodically by +470 mV. Similarly, comparison of $E_{1/2}$ for cyclam-ligated **5** versus $E_{1/2}$ for cyclam-ligated **7** shows that replacement of Fe^{2+} with Co^{2+}, within an identical ligand environment, causes the potential to shift cathodically by +765 mV. These differences reflect differences in ionization potentials for the two metals, and follow expected periodic trends. As demonstrated by the lower energy charge transfer bands in their electronic absorption spectra (vide supra), the Co^{2+} d-orbitals lie lower in energy than the Fe^{2+} orbitals making Co^{2+} more difficult to oxidize. Given this, Co^{2+} would not be the metal ion of choice for metalloenzymes, such as SOR, that function as reducing agents.

Comparison of the redox potentials ($E_{1/2}$; Table 3) of **8** versus those of **5** and **1**, shows that a cathodic shift in the redox potential by +275 mV upon replacement of primary amines with secondary amines, and +610 mV upon replacement of primary amines with tertiary amines. Tertiary amines stabilize iron in the +2 oxidation state, whereas primary amines stabilize iron in the +3 oxidation state, and secondary amines fall somewhere in between. One would expect the opposite trend on the basis of their relative bond lengths and Lewis basicities.

Comparison of the redox potential ($E_{1/2}$; Table 3) of **1** versus that of **3**, shows that the replacement of a thiolate sulfur (X in Table 2) with an amine nitrogen causes the potential to shift cathodically, by +503 mV. In contrast, replacement of the thiolate sulfur in **1** with an alkoxide oxygen in **2** causes the potential to shift in the opposite direction. The redox potential of the water-ligated alkoxide complex **2** (Scheme 1) is pH-dependent, shifting anodically by ~60 mV/pH unit, most likely because the coordinated water readily deprotonates.[28] Although the ligands are conserved with only minor changes to the apical X-atom, the coordination numbers differ for **1** (5-coordinate) versus **2** (6-coordinate) and **3** (6-coordinate), making these comparisons somewhat less valid. One would expect the redox potential to shift anodically in response to an increase in coordination number, implying that **3** would have an even more cathodically shifted potential in the absence of the sixth (Cl^-) ligand. Alkoxide-ligated **2** would have a less anodically shifted potential in the absence of its sixth (H_2O) ligand. Another property influencing redox potentials is overall molecular charge. Molecular charge is conserved for **1**, **2**, and **3** – all are monocations. This would not be the case for **2** at higher pH where deprotonation of the water would afford a neutral hydroxide-bound species, or for **3** in the absence of the Cl^- ligand where instead a dicationic (2+) species would form.

In summary, comparison of redox potentials indicates that the tertiary amine tren-ligands of **3** and **8** stabilize iron in the +2 oxidation state, whereas the alkoxide tren-ligand stabilizes iron in the +3 oxidation state. The primary amine thiolate tren-ligand falls somewhere in between, favoring the +3 oxidation state more than the amine, but less than an alkoxide. Thiolate-ligated $[Fe^{II}(S^{Me2}N_4(tren))]^+$ (**1**) is a better reducing agent than thiolate-ligated $[Co^{II}(S^{Me2}N_4(tren))]^+$ (**4**), and the ligand stabilizes iron in the +3 oxidation state, and cobalt in the +2 oxidation state. Within the cyclam-ligated series **5**–**7** similar trends are observed. Replacement of the apical thiolate of $[Fe^{II}(cyclam\text{-}PrS)]^+$ (**5**) with an apical alkoxide in $[Fe^{II}(cyclam\text{-}PrO)]^+$ (**6**) causes the redox potential to shift anodically by −100 mV, and replacement of the Fe^{2+} ion of **5** with a Co^{2+} ion (in **7**) causes the redox potential to shift cathodically by +765 mV.

3.5. Summary and conclusions

Comparison of the structurally-related derivatives described herein, and elsewhere [23,26,43], shows that thiolate ligands reduce metal ion Lewis acidity relative to alkoxides and amines, and have a strong *trans* influence thereby helping to maintain an open coordination site. With an open coordination site, the metal ion is accessible so that substrates can react via an inner sphere mechanism. Comparison of the redox potentials of the structurally analogous compounds described herein indicates that the higher-valent Fe^{3+} oxidation state is favored most by alkoxide ligands, and least by amine ligands. This fits with what one would expect based on the hard–soft acid–base classification of metal ions and ligands (Lewis acids and bases) [44]. Thiolates favor Fe^{3+} more than amines but less than alkoxides. This is somewhat surprising given that sulfur is usually considered to be a soft Lewis base, and Fe^{3+} a hard Lewis acid. As shown previously however [45], extensive π-interaction and delocalization stabilizes the Fe(III)–S bonds more than one would anticipate. For a redox active iron enzyme to function as a catalyst capable of reducing substrates, both the Fe^{3+} and the Fe^{2+} states must be accessible. Although a catalyst with a more anodic potential would be a more potent reducing agent, an excessively anodic potential would result in an inaccessible catalytically active reduced Fe^{2+} state [46]. Since an open coordination site, and a moderately low redox-potential

are both necessary for efficient, inner sphere, substrate (e.g superoxide) reduction to occur, the combination of a thiolate (as opposed to an alkoxide or amine) coordinated to iron (as opposed to cobalt), with primary (as opposed to secondary or tertiary) amines in the synthetic models creates both of these optimum conditions needed for this chemistry to occur. This implies that the cysteinate ligand of the non-heme iron enzyme SOR plays an important role in promoting function.

Acknowledgement

We thank Ed Solomon and his group for a very fruitful and synergistic ongoing collaboration. This work was supported by the NIH (Grant Number: GM 45811-17).

Appendix A. Supplementary material

Supplementary data associated with this article can be found, in the online version, at doi:10.1016/j.ica.2007.07.038.

References

[1] E.I. Solomon, Inorg. Chem. 45 (2006) 8012.
[2] J.A. Kovacs, Chem. Rev. 104 (2004) 825.
[3] P.V. Rao, R.H. Holm, Chem. Rev. 104 (2004) 527.
[4] H.B. Gray, B. Malström, R.J.P. Williams, J. Biol. Inorg. Chem. 5 (2000) 551.
[5] P.A. Lindahl, Biochemistry 41 (2002) 2097.
[6] P.V. Rao, S. Bhaduri, J. Jiang, D. Hong, R.H. Holm, J. Am. Chem. Soc. 127 (2005) 1933.
[7] J.V. Rodrigues, I.A. Abreu, D. Cabelli, M. Teixeira, Biochemistry 45 (2006) 9266.
[8] D.M. Kurtz Jr., Acc. Chem. Res. 37 (2004) 902.
[9] A.T. Fiedler, P.A. Bryngelson, M.J. Maroney, T.C. Brunold, J. Am. Chem. Soc. 127 (2005) 5449.
[10] J. Wuerges, J.-W. Lee, Y.-I. Yim, H.-S. Yim, S.-O. Kang, K.D. Carugo, Proc. Natl. Acad. Sci. USA 101 (2004) 8569.
[11] J. Shearer, L.M. Long, Inorg. Chem. 45 (2006) 2358.
[12] I.G. Denisov, T.M. Makris, S.G. Sligar, I. Schlichting, Chem. Rev. 105 (2005) 2253.
[13] H. Ogata, S. Hirota, A. Nakahara, H. Komori, N. Shibata, T. Kato, K. Kano, Y. Higuchi, Structure 13 (2005) 1635.
[14] P.T.R. Rajagopalan, X.C. Yu, D. Pei, J. Am. Chem. Soc. 119 (1997) 12418.
[15] S. Chang, V.V. Karambelkar, R.C. diTargiani, D.P. Goldberg, Inorg. Chem. 40 (2001) 194.
[16] L.M. Brines, J. Shearer, J.K. Fender, D. Schweitzer, S.C. Shoner, D. Barnhart, W. Kaminsky, S. Lovell, J.A. Kovacs, Inorg. Chem 46, in press.
[17] D.W. Randall, S.D. George, B. Hedman, K.O. Hodgson, K. Fujisawa, E.I. Solomon, J. Am. Chem. Soc. 122 (2000) 11620.
[18] T. Glaser, B. Hedman, K.O. Hodgson, E.I. Solomon, Acc. Chem. Res. 33 (2000) 859.
[19] S.D. George, M. Metz, R.K. Szilagyi, H. Wang, S.P. Cramer, Y. Lu, W.B. Tolman, B. Hedman, K.O. Hodgson, E.I. Solomon, J. Am. Chem. Soc. 123 (2001) 5757.
[20] M.D. Lowery, J.A. Guckert, M.S. Gebhard, E.I. Solomon, J. Am. Chem. Soc. 115 (1993) 3012.
[21] S. Shoner, D. Barnhart, J.A. Kovacs, Inorg. Chem. 34 (1995) 4517.
[22] H.L. Jackson, S.C. Shoner, D. Rittenberg, J.A. Cowen, S. Lovell, D. Barnhart, J.A. Kovacs, Inorg. Chem. 40 (2001) 1646.
[23] J.J. Ellison, A. Nienstedt, S.C. Shoner, D. Barnhart, J.A. Cowen, J.A. Kovacs, J. Am. Chem. Soc. 120 (1998) 5691.
[24] T. Kitagawa, A. Dey, P. Lugo-Mas, J. Benedict, W. Kaminsky, E. Solomon, J.A. Kovacs, J. Am. Chem. Soc. 128 (2006) 14448.
[25] J. Shearer, I.Y. Kung, S. Lovell, W. Kaminsky, J.A. Kovacs, J. Am. Chem. Soc. 123 (2001) 463.
[26] J. Shearer, H.L. Jackson, D. Schweitzer, D.K. Rittenberg, T.M. Leavy, W. Kaminsky, R.C. Scarrow, J.A. Kovacs, J. Am. Chem. Soc. 124 (2002) 11417.
[27] J. Shearer, J. Nehring, W. Kaminsky, J.A. Kovacs, Inorg. Chem. 40 (2001) 5483.
[28] L.M. Brines, W. Kaminsky, M.L. Kirk, J.A. Kovacs, 2007, manuscript in preparation.
[29] R.M. Theisen, J. Shearer, W. Kaminsky, J.A. Kovacs, Inorg. Chem. 43 (2004) 7682.
[30] D.D. Perrin, W.L.F. Armarego, D.R. Perrin, Purification of Laboratory Chemicals, 2nd ed., Pergamon Press, Elmsford, NY, 1980.
[31] D.H. Live, S.I. Chan, Anal. Chem. 42 (1970) 791.
[32] D.A. Evans, J. Chem. Soc. (1959) 2005.
[33] A.L. Van Geet, Anal. Chem. 40 (1968) 2227.
[34] J. Shearer, I. Kung, S. Lovell, J.A. Kovacs, Inorg. Chem. 39 (2000) 4998.
[35] D.V. Yandulov, R.R. Schrock, J. Am. Chem. Soc. 124 (2002) 6252.
[36] J.M. Smith, A.R. Sadique, T.R. Cundari, K.R. Rodgers, G. Lukat-Rodgers, R.J. Lachicotte, C.J. Flaschenriem, J. Vela, P.L. Holland, J. Am. Chem. Soc. 128 (2006) 756.
[37] B.J. O'Keefe, L.E. Breyfogle, M.A. Hillmyer, W.B. Tolman, J. Am. Chem. Soc. 124 (2002) 4384.
[38] S.D. Brown, T.A. Betley, J.C. Peters, J. Am. Chem. Soc. 125 (2003) 322.
[39] R.D. Shannon, Acta. Crystallogr., Sect. A 32 (1976) 751.
[40] R.M. Theisen, Ph.D. thesis, University of Washington, 2005.
[41] R.D. Swartz, J.A. Kovacs, manuscript in preparation.
[42] J. Shearer, R.C. Scarrow, J.A. Kovacs, J. Am. Chem. Soc. 124 (2002) 11709.
[43] S.C. Shoner, A. Nienstedt, J.J. Ellison, I. Kung, D. Barnhart, J.A. Kovacs, Inorg. Chem. 37 (1998) 5721.
[44] S.J. Lippard, J.M. Berg, Principles of Bioinorganic Chemistry, University Science, Mill Valley, 1994.
[45] P. Kennepohl, F. Neese, D. Schweitzer, H.L. Jackson, J.A. Kovacs, E.I. Solomon, Inorg. Chem. 44 (2005) 1826.
[46] J. Shearer, S.B. Fitch, W. Kaminsky, J. Benedict, R.C. Scarrow, J.A. Kovacs, Proc. Natl. Acad. Sci., USA 100 (2003) 3671.